

Numerical simulations of compressible Rayleigh–Taylor turbulence in stratified fluids

To cite this article: A Scagliarini *et al* 2010 *Phys. Scr.* **2010** 014017

View the [article online](#) for updates and enhancements.

Related content

- [Second order closure for stratified convection: bulk region and overshooting](#)
L Biferale, F Mantovani, M Pivanti et al.
- [Front propagation in Rayleigh-Taylor systems with reaction](#)
A Scagliarini, L Biferale, F Mantovani et al.
- [Reactive Rayleigh-Taylor systems: Front propagation and non-stationarity](#)
L. Biferale, F. Mantovani, M. Sbragaglia et al.

Recent citations

- [A comparative study of approaches for modeling Rayleigh–Taylor turbulent mixing](#)
Snezhana I Abarzhi and Robert Rosner

Numerical simulations of compressible Rayleigh–Taylor turbulence in stratified fluids

A Scagliarini^{1,2}, L Biferale^{1,2}, M Sbragaglia¹, K Sugiyama³ and F Toschi^{2,4}

¹ Department of Physics and INFN, University of Tor Vergata, Via della Ricerca Scientifica 1, 00133 Rome, Italy

² International Collaboration for Turbulence Research

³ Department of Mechanical Engineering, School of Engineering, The University of Tokyo, 7-3-1, Hongo, Bunkyo-ku, Tokyo 113-8656, Japan

⁴ Department of Physics and Department of Mathematics and Computer Science, Eindhoven University of Technology, 5600 MB Eindhoven, The Netherlands

E-mail: andrea.scagliarini@roma2.infn.it

Received 31 May 2010

Accepted for publication 18 October 2010

Published 31 December 2010

Online at stacks.iop.org/PhysScr/T142/014017

Abstract

We present the results of our numerical simulations of the Rayleigh–Taylor turbulence, performed using a recently proposed (Sbragaglia *et al* 2009 *J. Fluid Mech.* **628** 299, Scagliarini *et al* 2010 *Phys. Fluids* **22** 055101) lattice Boltzmann method that can describe consistently a thermal compressible flow subjected to an external forcing. The method allowed us to study the system in both the nearly Boussinesq regime and the strongly compressible regime. Moreover, we show that when the stratification is important, the presence of the adiabatic gradient causes the arrest of the mixing process.

PACS numbers: 47.20.Bp, 47.55.Hd, 47.11.St, 42.27.E–

1. Introduction

Computational methods based on discrete-velocity models have attracted considerable interest in recent years as efficient tools for the theoretical investigation of the properties of complex flows [3–7]. In particular, it has been recently shown that an important class of these models, known as the lattice Boltzmann models (LBM) [8–10], can be derived from the continuum Boltzmann (BGK) equation [11]. This derivation involves the expansion in suitable Hermite polynomials of the distribution functions $f(\mathbf{x}, \boldsymbol{\xi}, t)$, describing the probability of finding a molecule at the space–time location (\mathbf{x}, t) and with velocity $\boldsymbol{\xi}$ [5, 12–14]. Therefore, the corresponding lattice dynamics are well founded in terms of an underlying continuum kinetic theory. The state of the art is satisfactory concerning iso-thermal flows, even in the presence of complex bulk physics (multi-phase, multi-component) [3, 4, 15] and/or with complex boundary properties including roughness, wetting and slip boundary conditions [16–18]. The situation is much less satisfactory when hydrodynamical temperature fluctuations play an active role in the flow evolution, due

to complex compressible effects or to phase transition in multi-phase systems.

Within this framework, we recently developed [1, 2] a new LBM that allows us to incorporate the effects of external/internal forces into thermal systems. Here, we use this new algorithm to study highly compressible Rayleigh–Taylor (RT) systems, with an initial configuration such that two blobs of the same fluid are prepared with two different temperatures (hot, less dense and blob below, cold, denser, blob above). We show that the method is able to handle the highly non-trivial spatiotemporal evolution of the system even in the developing turbulent phase. In this case, we could push the numerics up to Atwood numbers $At \sim 0.4$. The maximum Rayleigh numbers achieved are $Ra \sim 4 \times 10^{10}$ for $At = 0.05$ and $Ra \sim 2 \times 10^9$ for $At = 0.4$. This paper is organized as follows. We will first describe the method (section 2), the numerical setup (section 3) and the system studied (section 4); then we will discuss the two main physical results, namely the stratification (section 5) and compressibility (section 6) effects, and some features related to the conservation of mean quantities (section 7). Our conclusions are presented in section 8.

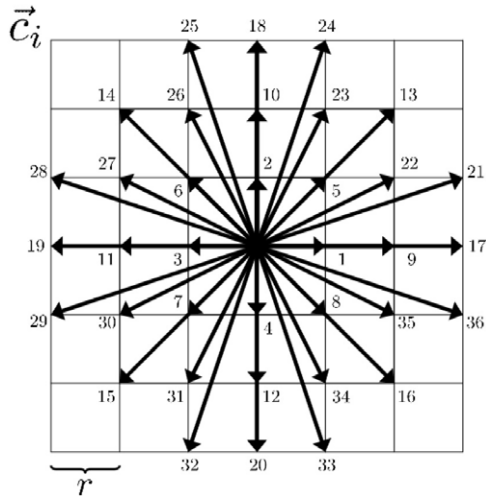


Figure 1. Scheme of the discrete set of velocities; r is the lattice constant whose value is approximately $r = 1.1969$ (see [2] and references therein).

2. The lattice Boltzmann model

Here we introduce the simulated equation set, along with a brief description of the computational lattice Boltzmann method employed. More details, along with many validations, can be found in [2]. The thermal-kinetic description of a compressible gas/fluid of variable density ρ , local velocity \mathbf{u} and internal energy \mathcal{K} and subject to a local body force density \mathbf{g} is given by the following equations:

$$\begin{aligned} \partial_t \rho + \partial_i (\rho u_i) &= 0, \\ \partial_t (\rho u_k) + \partial_i (P_{ik}) &= \rho g_k, \\ \partial_t \mathcal{K} + \frac{1}{2} \partial_i q_i &= \rho g_i u_i, \end{aligned} \quad (1)$$

where P_{ik} and q_i are the momentum and energy fluxes describing advection, viscous properties and thermal diffusivities in the hydrodynamical limit.

In [1], it has been shown that it is possible to recover exactly these equations, starting from a continuum Boltzmann equation and introducing a suitable shift of the velocity and temperature fields entering the local equilibrium.

The lattice counterpart of the continuum description can be obtained through the lattice Boltzmann discretization ($f_i(\mathbf{x}, t)$ are the fields associated with the populations),

$$f_i(\mathbf{x} + \mathbf{c}_i \Delta t, t + \Delta t) - f_i(\mathbf{x}, t) = -\frac{\Delta t}{\tau_{\text{LBM}}} (f_i(\mathbf{x}, t) - f_i^{(\text{eq})}), \quad (2)$$

where the equilibrium $f_i^{(\text{eq})}$ is expressed in terms of hydrodynamical fields and the body force term \mathbf{g} , and the subscript i runs over the discrete set of velocities \mathbf{c}_i (see figure 1); in equation (2) τ_{LBM} is the relaxation time (which is related to the dynamic viscosity ν via $\nu = \rho T (\tau_{\text{LBM}} - 1/2)$, T being the temperature field), and Δt the time step of the simulation.

The macroscopic fields (density, momentum and temperature) are defined in terms of the lattice Boltzmann populations: $\rho = \sum_i f_i$, $\rho \mathbf{u} = \sum_i \mathbf{c}_i f_i$, $D\rho T = \sum_i |\mathbf{c}_i - \mathbf{u}|^2 f_i$. Lattice discretization induces non-trivial correction terms in the macroscopic evolution of averaged

hydrodynamical quantities. In particular, both momentum and temperature must be renormalized by discretization effects in order to recover the correct description out of the discretized LBM variables: the first correction to momentum is given by the pre- and post-collisional average [19, 20] $\mathbf{u}^{(\text{H})} = \mathbf{u} + \frac{\Delta t}{2} \mathbf{g}$ and the first, non-trivial correction to the temperature field is given by [1] $T^{(\text{H})} = T + \frac{(\Delta t)^2 g^2}{4D}$ (D is the dimensionality of the system). Using these ‘renormalized’ hydrodynamical fields it is possible to recover, through a Taylor expansion in Δt , the thermo-hydrodynamical equations [1, 2],

$$D_t \rho = -\rho \partial_i u_i^{(\text{H})}, \quad (3)$$

$$\rho D_t u_i^{(\text{H})} = -\partial_i p - \rho g \delta_{i,3} + \nu \partial_{jj} u_i^{(\text{H})}, \quad (4)$$

$$\rho c_v D_t T^{(\text{H})} + p \partial_i u_i^{(\text{H})} = k \partial_{ii} T^{(\text{H})}, \quad (5)$$

where we have introduced the material derivative, $D_t = \partial_t + u_j^{(\text{H})} \partial_j$, and we have neglected viscous dissipation in the temperature equation (usually small). Moreover, c_v is the specific heat at constant volume for an ideal gas $p = \rho T^{(\text{H})}$, and ν and k are the transport coefficients. From now on, for the sake of simplicity, we will drop the superscript (H), knowing that we are dealing with lattice hydrodynamical quantities satisfying equations (3)–(5). As a tool for the numerical simulation of systems such as (or similar to) the one we plan to study, the LBM may suffer, in principle, from some issues, such as having too high Mach numbers and too low viscosity (i.e. very small relaxation time, which is undesirable especially in the presence of processes very far from local equilibrium): we could, however, check the accuracy of our method against different methods, finding it extremely competitive, within the range of parameters discussed in this paper [21].

3. Details of the numerical simulations

We use a two-dimensional (2D) LBM algorithm, with 37 population fields (a so-called D2Q37 model), moving with the lattice speeds shown in figure 1. Since the lattice spacing can be taken to be unitary, the time step Δt will be the inverse of the lattice unit speed, i.e. $\Delta t \sim 0.835$ [2]. Three different kinds of simulations have been performed (whose parameters are summarized in table 1): (A) with a large enough adiabatic gradient (but small Atwood number) in order to address the stratification effects on the mixing layer growth, while still being very close to the Boussinesq approximation; (B) with an adiabatic gradient that is twice the one of run A; (C) with large Atwood number in order to describe compressibility effects, outside the Boussinesq regime, but far from the adiabatic profile; (D) with small adiabatic gradient and small Atwood number.

4. The RT system

Superposition of a heavy fluid above a lighter one in a constant acceleration field depicts a hydrodynamic unstable configuration called the RT instability [22] with applications in different fields ranging from inertial-confinement

Table 1. Parameters for the three types of RT runs. Key: Atwood number, $At = (T_d - T_u)/(T_d + T_u)$; viscosity, $\nu = \rho T (\tau_{\text{LBM}} - 1/2)$; gravity, g ; temperature in the upper half region, T_u ; temperature in the lower half region, T_d ; normalization time, $\tilde{\tau} = \sqrt{L_x/(g At)}$. The average density value is 1. All entries are in natural lattice Boltzmann units.

	At	L_x	L_z	$\tau_{\text{LBM}} - 0.5$	g	T_u	T_d	$\tilde{\tau}$
Run A	0.05	800	1400	0.001	2.5×10^{-4}	0.95	1.05	8×10^3
Run B	0.05	800	1400	0.001	5×10^{-4}	0.95	1.05	5.6×10^3
Run C	0.4	1664	4400	0.1	1×10^{-4}	0.6	1.4	6.5×10^3
Run D	0.05	1024	2400	0.005	5×10^{-5}	0.95	1.05	2×10^4

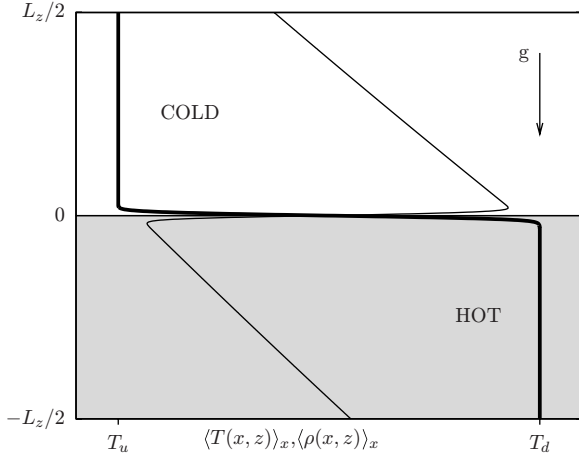


Figure 2. Initial condition of the RT system, as given by equation (7). We show the mean temperature (bold line) and density (thin line) profiles as a function of the z -coordinate (on the vertical axis).

fusion [23] to supernovae explosions [24] among many others [25]. Although this instability was studied for decades it is still an open problem in several aspects [26]. In particular, it is crucial to control the initial and late evolution of the mixing layer between the two miscible fluids; the small-scale turbulent fluctuations, their anisotropic/isotropic ratio; their dependence on the initial perturbation spectrum or on the physical dimensions of the embedding space [27, 28]. In many cases, especially concerning astrophysical and nuclear applications, the two fluids evolve with strong compressible and/or stratification effects, a situation that is difficult to investigate either theoretically or numerically. Here, we concentrate on the large-scale properties of the mixing layer, studying a slightly different RT system than is usually found in the literature: the spatiotemporal evolution of a single-component fluid when initially prepared in hydrostatic unstable equilibrium, i.e. with a cold uniform region in the top half and a hot uniform region on the bottom half (see figure 2) in analogy with natural convection. For the sake of simplicity we limit the investigation to the 2D case. While small-scale fluctuations may be strongly different in 2D or 3D geometries, the large-scale mixing layer growth is not supposed to change its qualitative evolution [29, 30]. Gray-scale coded snapshots of a typical RT evolution are shown in figure 3, showing all the complexity of the phenomena. Let us start to define precisely the initial setup. We prepare a single-component compressible flow in a 2D tank of size $L_x \times L_z$, with adiabatic and no-slip boundary conditions on the top and bottom walls and with periodic boundary conditions on the vertical boundaries. For convenience we define the initial interface to be at height $z = 0$, the box extending up to

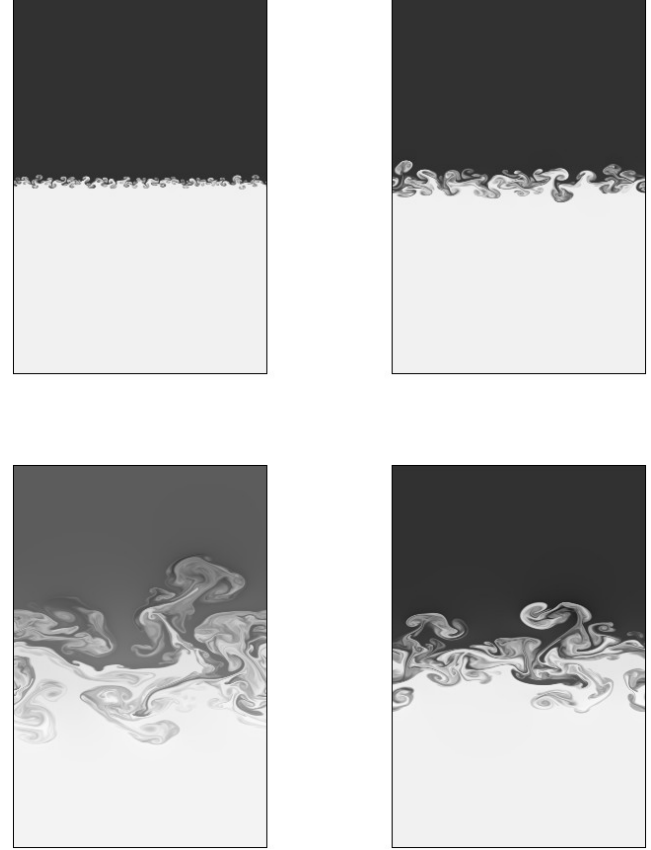


Figure 3. Spatiotemporal evolution for a typical RT run with $L_x \times L_z = 1024 \times 2400$, $T_u = 0.95$, $T_d = 1.05$ at four instants of time: $t = \tilde{\tau}$, $2\tilde{\tau}$, $4\tilde{\tau}$ and $6\tilde{\tau}$ (run D in table 1) going clockwise from the top left panel.

$z = L_z/2$ above and $z = -L_z/2$ below it (see figure 2). In the two half volumes, we then fix two different homogeneous temperatures, with the corresponding hydrostatic density profiles, ρ_0 , verifying

$$\partial_z p_0(z) = -g\rho_0(z). \quad (6)$$

Considering that in each half we have $p_0(z) = T\rho_0(z)$, with T fixed, the solution has exponentially decaying behavior in the two half volumes, each one driven by its own temperature value. The initial hydrostatic unstable configuration is therefore given by

$$\begin{aligned} T_0(z) &= T_u; & \rho_0(z) &= \rho_u \exp(-g(z - z_c)/T_u); & z > 0 \\ T_0(z) &= T_d; & \rho_0(z) &= \rho_b \exp(-g(z - z_c)/T_d); & z < 0. \end{aligned} \quad (7)$$

To be at equilibrium, we require to have the same pressure at the interface, $z = z_c = 0$, which translates into a simple condition on the prefactor of the above expressions:

$$\rho_u T_u = \rho_b T_d. \quad (8)$$

Because $T_u < T_d$, we have at the interface $\rho_u > \rho_b$. As far as we know, there are no exhaustive detailed calculations of the stability problem for such a configuration, even though not too different from the usual RT compressible case [22, 31, 32]. As mentioned before, this is not the common way to study RT systems, which is usually meant as the superposition of two different miscible fluids, isothermal, with different densities [22, 27, 31, 33]. As long as compressible effects are small, one may safely neglect pressure fluctuations and write, for the case of an ideal gas,

$$\frac{\delta\rho}{\rho} \sim -\frac{\delta T}{T} \quad (9)$$

and the two RT experiments are then strictly equivalent. Moreover, in the latter case, if one neglects the dependence of viscosity and thermal diffusivity on temperature, the final evolution is indistinguishable from the evolution of temperature in the Boussinesq approximation [28, 29].

5. The adiabatic gradient and the arrest of the mixing process

The main novelty in the system investigated here is due to the presence of new effects induced by the adiabatic gradient, which can be written for an ideal gas as $\beta_{ad} = g/c_p$. The role of stratification, i.e. of the adiabatic gradient, is quite well established in the context of Rayleigh–Bénard convection (see e.g. [34]), whereas it has only in recent years been studied, both numerically [35, 36] and theoretically [37, 38], in a setup such as that of RT mixing. In order to understand the main physical point it is useful to consider the RT mixing layer as equivalent to a (developing) Rayleigh–Bénard system with an imposed mean temperature gradient [39, 40]. Let us designate by $L_{ml}(t)$ the typical width of the RT mixing layer at a given time as measured, for example, from the distance between the two elevations where the mean temperature profile is 1% lower or higher than the bottom and top, respectively, unmixed temperature values, $L_{ml} = z_u - z_d$, where $\langle T(x, z_u) \rangle_x = 1.01T_u$ and $\langle T(x, z_d) \rangle_x = 0.99T_d$. The temperature tends to develop a linear profile inside the mixing region, the resulting instantaneous temperature gradient being given by $\beta(t) = (T_d - T_u)/L_{ml}(t)$ and hence decreasing in time inversely to the growth of the mixing length. As a result, at a certain time (if the box is high enough) the instantaneous temperature gradient will become of the same order as the adiabatic gradient, $\beta(t) \sim \beta_{ad}$ and the growth of the mixing length will stop. In figure 4 we show the mean temperature profiles once the mixing has already stopped, for two different values of gravity (runs A and B in table 1): in the mixing layer the two curves have developed a linear profile with slope g/c_p , which is exactly the adiabatic gradient for an ideal gas. One can define an instantaneous Rayleigh number, driving the physics inside the mixing layer, as

$$\tilde{Ra}(t) = \frac{(g/\tilde{T}_0)L_{ml}^4(t)(\beta(t) - \beta_{ad})}{(k/\tilde{\rho}_0 c_p)(\nu/\tilde{\rho}_0)}, \quad (10)$$

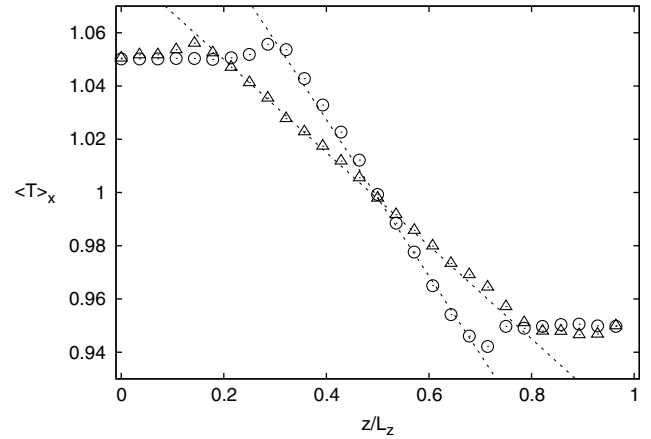


Figure 4. Mean temperature profiles $\langle T \rangle_x(z, t)$ for run A (Δ) and run B (\odot), in a stage where the mixing process has already stopped ($t \simeq 13\bar{\tau}$ for both cases). The dashed lines represent the corresponding adiabatic profiles.

where $\tilde{(\cdot)}$ indicates quantities evaluated in the middle layer. It is clear that for small times, $\beta(t) \ll \beta_{ad}$, the effective instantaneous Rayleigh number is high: the system is unstable, and the mixing length grows. On the other hand, as time elapses, the vertical mean temperature gradient decreases until a point when $\beta(t) \sim \beta_{ad}$, the instantaneous effective Rayleigh number becomes $Ra(t) \sim \mathcal{O}(1)$ and the system tends to be stabilized. We can then identify an *adiabatic length*,

$$L_{ad} = (T_d - T_u)/\beta_{ad} = c_p \Delta T/g,$$

which determines the maximum length achievable by the mixing layer, in our configuration. When the mean temperature approaches the adiabatic profile, the system shows a sudden slowing down of the growth of the mixing layer, which eventually stops. A possible way of estimating quantitatively when and how the adiabatic gradient starts to play a role in the growth of the mixing layer width $L_{ml}(t)$ is to use a simple phenomenological closure for large-scale quantities in the system. We start from the self-similar scaling predicted by [41, 42] for the homogeneous unstratified growth,

$$(\dot{L}_{ml}(t))^2 = 4\alpha g At L_{ml}(t), \quad (11)$$

which has a unique solution in terms of the initial value, $L_{ml}(t_0)$,

$$L_{ml}(t) = L_{ml}(t_0) + 2\sqrt{\alpha At g} (t - t_0) + \alpha At g (t - t_0)^2. \quad (12)$$

In order to minimally modify the above expression considering the saturation effects induced by stratification, we proposed to use in [2]

$$(\dot{L}_{ml}(t))^2 = 4\alpha g At L_{ml}(t) \psi \left(\frac{L_{ml}(t)}{L_{ad}} \right), \quad (13)$$

where $\psi = \psi(x)$ must be a function fulfilling the condition $\psi \rightarrow 1$ as $x \rightarrow 0$ (that is, for $L_{ad} \rightarrow \infty$), in order to recover equation (11) for the unstratified case when the adiabatic gradient goes to zero. We further add the requirement

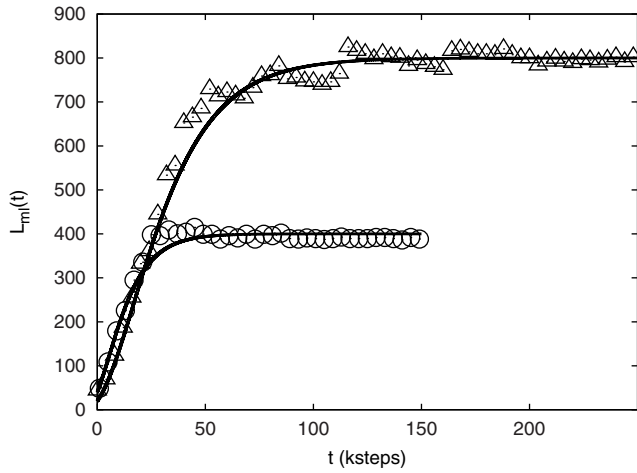


Figure 5. Evolution of the mixing layer, $L_{ml}(t)$, versus time with two different adiabatic lengths, corresponding to run A (Δ) and run B (\odot) in table 1. Solid bold lines correspond to the theoretical prediction (13) with $\alpha = 0.05$.

of reaching the adiabatic profile with zero velocity and acceleration, enforcing a strict irreversible growth, i.e. $\dot{L}_{ml} \geq 0$, as it must be for the case of miscible fluids. Under these assumptions it can be shown that the simplest form of the function ψ is

$$\psi\left(\frac{L}{L_{ad}}\right) = C \left[e^{-(L-L_{ad}/L_{ad})} - \left(\frac{2L_{ad}-L}{L_{ad}}\right) \right], \quad (14)$$

where the prefactor C must be set equal to $1/(e-2)$ to comply with the prescribed boundary conditions. Equation (13) must be considered as a zeroth order phenomenological way of taking into account the adiabatic gradient in the mixing layer evolution. We integrated numerically equation (13) testing the result in figure 5, where we show that it is possible to fit the global evolution of the mixing length $L_{ml}(t)$, by using reasonable [26] values of α , for all times, including the long-time behavior where $L_{ml}(t) \sim L_{ad}$. We can then interpret the solution of our equation (13) as a good generalization of (12) including also the adiabatic gradient effects.

6. Effects of compressibility

In this section, we are going to study the effects of flow compressibility on the dynamics of an RT system for varying Atwood number. To do that, we come back to the discussion sketched in section 4; since the equation of state for our fluid is that of a perfect gas, the pressure, temperature and density fluctuations are related by

$$\frac{\delta P}{P} = \frac{\delta \rho}{\rho} + \frac{\delta T}{T}. \quad (15)$$

Hence, as discussed in section 4, if pressure fluctuations are small, density fluctuations are linearly slaved on those of temperature, which will also be small, and the system behaves as a Boussinesq fluid. Conversely, if the temperature jump is high there will be large density differences through system (7) and hence large pressure fluctuations (6); thus we expect that, on increasing the Atwood number, the dynamics become

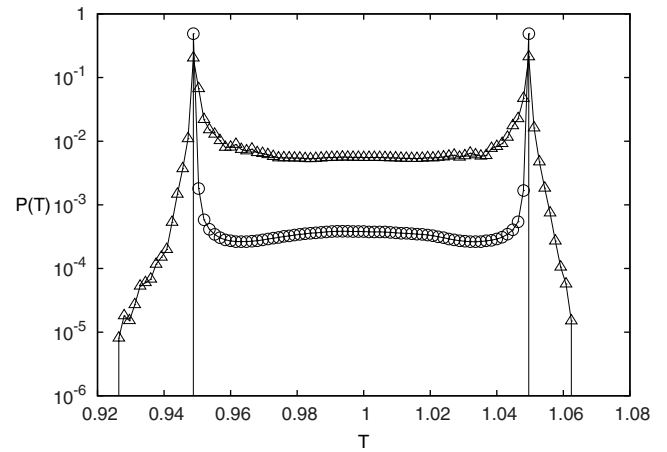


Figure 6. PDFs of temperature at $t = \tilde{\tau}$ (\odot) and $t = 5\tilde{\tau}$ (Δ), for $At = 0.05$, for which the flow is basically Boussinesq like.

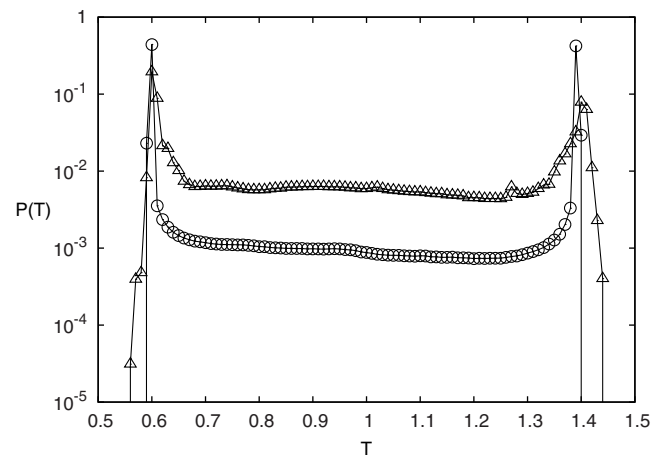


Figure 7. PDFs at $t = \tilde{\tau}$ (\odot) and $t = 5\tilde{\tau}$ (Δ), for $At = 0.4$, that is, in the highly compressible regime.

more and more compressible and pressure turns out to be a dynamically relevant variable.

We show, first, how the mixing acts on the statistics of the (pointwise) temperature; as one can see in figures 6 and 7, where we plot the probability density function (PDF) of temperature at two instants of time for $At = 0.05$ and $At = 0.4$ (for which the squared Mach number is $Ma^2 \sim 0.16$), the distribution has initially a bimodal character, since at the beginning the volume is divided into two homogeneous regions of hot and cold fluids. Due to the mixing, at later times, the probability of having intermediate values of temperature increases; however, the two peaks remain dominant, because the system dynamics do not yet involve the whole box and because the diffusive processes are so slow that they are irrelevant at this stage. No evident differences (except the obviously larger range of values spanned) emerge between the low and high Atwood number cases. Hence, to better address this point, we study the statistics of pressure fluctuations (with respect to the mean profile) in the two compressibility regimes; we define the fluctuation of the generic thermo-hydrodynamic field ϕ as

$$\delta\phi(\mathbf{x}, t) = \phi(\mathbf{x}, t) - \langle\phi\rangle_x(z, t); \quad \langle\phi\rangle_x(z, t) = \int_0^{L_x} \phi \, dx.$$

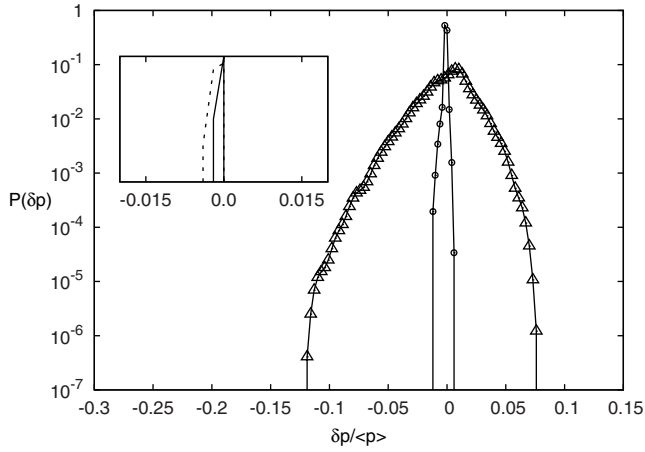


Figure 8. PDFs of pressure fluctuations at time $t = \bar{\tau}$ (\odot) and $t = 5\bar{\tau}$ (\triangle), for $At = 0.4$ and (inset) for $At = 0.05$ ($t = \bar{\tau}$, solid line, and $t = 5\bar{\tau}$, dashed line). Whereas in the low At case, the PDF remains basically a δ -function at any time, it is more spread (with tails becoming larger as time elapses) in the compressible case ($At = 0.4$).

In figure 8, we show the PDFs of δp , measured again inside the whole volume, at two different instants of time during the mixing process, for two Atwood numbers. It can be noted how the PDF, while being basically a δ -function for low At and remaining such at any time (see the inset of figure 8), is more spread at higher At and enlarges its tails as time elapses, confirming that the pressure dynamics is now highly non-trivial.

It is, moreover, known that increasing the degree of compressibility of the dynamics has also a strong impact on the stability properties of the system [43] and on the statistics of the mixing layer growth process, determining in the latter case an asymmetry in the growth of the mixing layer [43], noticeable also in the statistics of the growth parameter α [2]. We would like to discuss here such effects, without appealing to any phenomenological model, but in terms, again, of PDFs of the temperature field. The use of PDFs to address compressibility effects in RT was also suggested, although in a slightly different way, in [37, 44], in regimes from low ($Ma^2 \sim 0.008$) to moderately high ($Ma^2 \sim 0.1$) squared Mach number. With this aim, we measured the $\mathcal{P}(T)$ where $T = T(x, z^*, t^* = 5\bar{\tau})$ along lines at two fixed heights z^* (at a certain time in the late stage of the evolution), within the mixing layer, symmetrically displaced with respect to the mid-cell; in particular we chose $z^* = \pm L_{ml}(t)/2$. In figures 9 and 10, we plot the PDFs for such heights for $At = 0.05$ and $At = 0.4$, respectively. In both cases, of course, the PDF corresponding to the upper height shows a peak at lower values of T (close to the unmixed cold fluid value), and vice versa for the lower height. However, whereas for small At the two PDFs are symmetric with respect to the average temperature (in some sense they transform into each other upon reversal around $T = 1$), for the compressible case figure 10 displays a clear asymmetry, where the PDF measured at the lower z -location develops a more intense tail at low T values, indicating that falling cold fluid spikes are faster (and mix more slowly) than rising hot fluid bubbles.

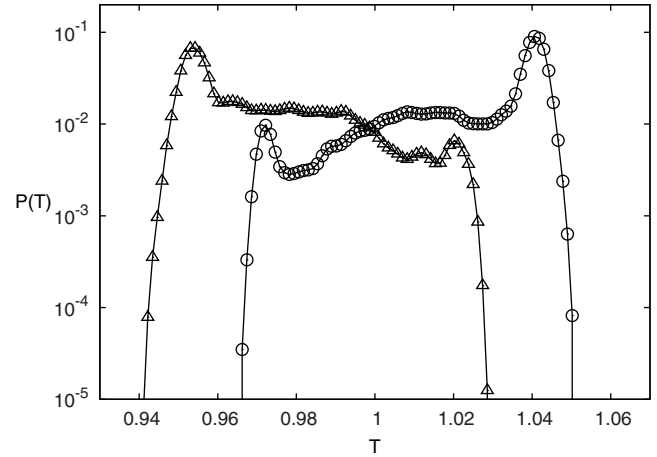


Figure 9. PDFs of the temperature field $T(x, z^*, t = 5\bar{\tau})$, measured at $z^* = \pm L_{ml}(t)/2$, for $At = 0.05$. The two PDFs show peaks close to the values of T of the unmixed cold (at $z^* = +L_{ml}/2$; \triangle) and hot (at $z^* = -L_{ml}/2$; \odot) fluids, respectively; the two PDFs are symmetric to each other with respect to the mean temperature value $T = 1$ (typical phenomenology for a Boussinesq system).

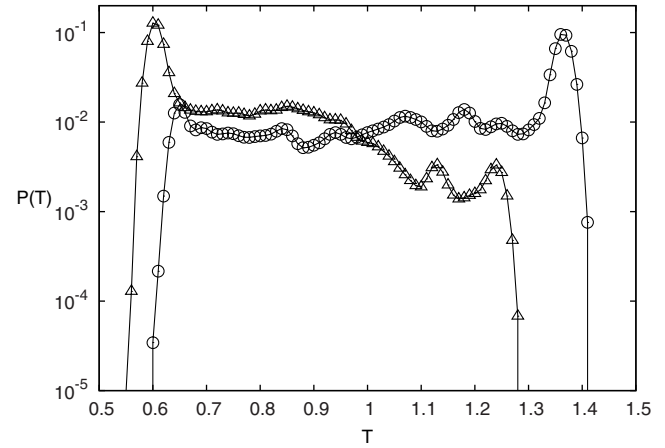


Figure 10. The same as figure 9 but for $At = 0.4$. In contrast to the Boussinesq (low At) case, the two PDFs are no longer symmetric, since the one measured at the lower height develops a fatter tail at low T values, indicating the asymmetry in the mixing process evolution.

7. Evolution of averaged quantities

If we integrate equation (4), multiplied by u_i , over the whole volume, since the boundary conditions are periodic at the vertical walls, and set zero velocity (no-slip) at the top and bottom plates, we obtain the following equation for the mean kinetic energy,

$$\partial_t \left\langle \frac{\rho u^2}{2} \right\rangle = \langle \rho g u_z \rangle - \epsilon_{\text{diss}}, \quad (16)$$

where $\langle \dots \rangle = 1/(L_x L_z) \int (\dots) dx dz$ denotes the space average, and $\epsilon_{\text{diss}} = \nu \langle (\partial_j u_i)^2 \rangle$. Equation (16) indicates that the total forcing, due to the gravitational field, is consumed partly by transformation into kinetic energy and partly by dissipation. In figure 11, we show the fraction of forcing transferred as kinetic energy ($(dE/dt)/\langle \rho g u_z \rangle$) and dissipated ($\epsilon_{\text{diss}}/\langle \rho g u_z \rangle$), and we observe that the latter is much smaller than the former, as one would have expected, the dissipation

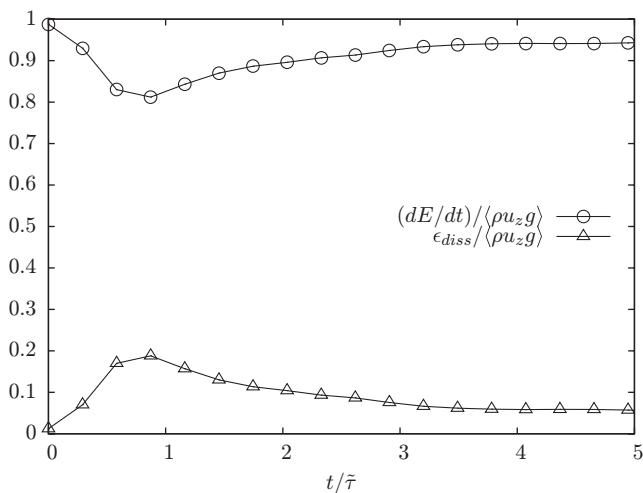


Figure 11. Time derivative of the kinetic energy (○) and dissipation (△) as functions of time, shown as fraction of the forcing term $\langle \rho g u_z \rangle$. Note that the forcing due to gravity is almost entirely converted into kinetic energy, since the dissipation is basically negligible in 2D turbulence.

being negligible in 2D. This behavior is in strong contrast with what happens in 3D, where energy is transferred downscale and a sort of equipartition between kinetic energy growth and energy dissipation is achieved [45, 46].

8. Conclusions

We simulated, by means of a new lattice Boltzmann algorithm, the turbulent dynamics of a Rayleigh–Taylor system, the characteristics of the method letting us tune the effects of both stratification and compressibility. Concerning the former problem, we discussed the importance of the adiabatic gradient for the growth of the RT mixing layer, showing the existence of the phenomenon of arrest of the mixing process and of a maximal width, the adiabatic length, L_{ad} , for the mixing region. We then measured the PDFs of density and temperature fluctuations inside the mixing region, observing that whereas the two statistics are almost identical for small Atwood numbers (negligible compressibility), they decouple when compressibility is large, owing to the increased relevance of pressure fluctuations, whose PDF we also measured, thus confirming that for large temperature jumps, pressure plays an active dynamical role.

Acknowledgments

We acknowledge the collaboration of R Tripiccione and F Mantovani for useful discussions and technical support. AS warmly thanks the TMB-2009 committee for assigning the ‘Young Scientist Award’ of the conference for the work he presented on Eulerian and Lagrangian statistics in incompressible and weakly compressible turbulence. The choice of submitting later this new material on RT turbulence was due to the fact that it is more recent and, we think, of possibly greater interest for the TMB community.

References

- [1] Sbragaglia M, Benzi R, Biferale L, Chen H, Shan X and Succi S 2009 Lattice Boltzmann method with self-consistent thermo-hydrodynamic equilibria *J. Fluid Mech.* **628** 299
- [2] Scagliarini A, Biferale L, Sbragaglia M, Sugiyama K and Toschi F 2010 Lattice Boltzmann methods for compressible flows: continuum limit and applications to Rayleigh–Taylor systems *Phys. Fluids* **22** 055101
- [3] Shan X and Chen H 1993 Lattice Boltzmann model for simulating flows with multiple phases and components *Phys. Rev. E* **47** 1815
- [4] Swift M R, Osborn W R and Yeomans J M 1995 Lattice Boltzmann simulation of nonideal fluids *Phys. Rev. Lett.* **75** 830
- [5] He X and Luo L S 1997 Theory of the lattice Boltzmann method: from the Boltzmann equation to the lattice Boltzmann equation *Phys. Rev. E* **56** 6811
- [6] Ladd A J C 1994 Numerical simulations of particulate suspensions via a discretized Boltzmann equation. 2. Numerical results *J. Fluid. Mech.* **271** 311
- [7] Duenweg B and Ladd A J C 2009 Lattice Boltzmann simulations of soft matter systems *Adv. Poly. Sci.* **221** 89–166
- [8] Wolf-Gladrow D 2000 *Lattice–Gas Cellular Automata and Lattice Boltzmann Models* (New York: Springer)
- [9] Benzi R, Succi S and Vergassola M 1992 The lattice Boltzmann equation: theory and applications *Phys. Rep.* **222** 145
- [10] Chen S and Doolen G 1998 Lattice Boltzmann method for fluid flows *Annu. Rev. Fluid Mech.* **30** 329
- [11] Bathnagar P-L, Gross E and Krook M 1954 A model for collision processes in gases *Phys. Rev.* **94** 511
- [12] Shan X and He X 1998 Discretization of the velocity space in the solution of the Boltzmann equation *Phys. Rev. Lett.* **80** 65
- [13] Martys N S, Shan X and Chen H 1998 Evaluation of the external force term in the discrete Boltzmann equation *Phys. Rev. E* **58** 6865
- [14] Shan X, Yuan F and Chen H 2006 Kinetic theory representation of hydrodynamics: a way beyond the Navier–Stokes equation *J. Fluid Mech.* **550** 413
- [15] He X and Doolen G 2001 Thermodynamic foundations of kinetic theory and lattice Boltzmann models for multiphase flows *J. Stat. Phys.* **107** 309
- [16] Benzi R, Biferale L, Sbragaglia M, Succi S and Toschi F 2006 Mesoscopic modelling of a two-phase flow in presence of the boundaries: the contact angle *Phys. Rev. E* **74** 021509
- [17] Sbragaglia M, Benzi R, Biferale L, Succi S and Toschi F 2006 Surface roughness–hydrophobicity coupling in microchannel and nanochannel flows *Phys. Rev. Lett.* **97** 204503
- [18] Hyvaluoma J and Harting J 2008 Slip flow over structured surfaces with entrapped microbubbles *Phys. Rev. Lett.* **100** 246001
- [19] Buick J M and Greated C A 2000 Gravity in a lattice Boltzmann model *Phys. Rev. E* **61** 5307
- [20] Guo Z, Zheng C and Shi B 2002 Discrete lattice effects on the forcing term in the lattice Boltzmann method *Phys. Rev. E* **65** 046308
- [21] Biferale L, Mantovani F, Sbragaglia M, Scagliarini A, Toschi F and Tripiccione R 2010 High resolution numerical study of Rayleigh–Taylor turbulence using a thermal lattice Boltzmann scheme *Phys. Fluids* **22** 115112
- [22] Chandrasekhar S 1961 *Hydrodynamic and Hydromagnetic Stability* (Oxford: Clarendon)
- [23] Lindl J D 1998 *Inertial Confinement Fusion* (New York: Springer)

- [24] Zingale M, Woosley S E, Rendleman C A, Day M S and Bell J B 2005 Three-dimensional numerical simulations of Rayleigh–Taylor unstable flames in type Ia supernovae *ApJ* **632** 1021
- [25] Sharp D H 1984 An overview of Rayleigh–Taylor instability *Physica D* **12** 3
- [26] Dimonte G *et al* 2004 A comparative study of the Rayleigh–Taylor instability using high-resolution three-dimensional numerical simulations: the Alpha group collaboration *Phys. Fluids* **16** 1668
- [27] Livescu D, Ristorcelli J R, Gore R A, Dean S H, Cabot W H and Cook A W 2009 High Reynolds numbers Rayleigh–Taylor turbulence *J. Turbul.* **10** 1–32
- [28] Boffetta G, Mazzino A, Musacchio S and Vozella L 2009 Kolmogorov scaling and intermittency in Rayleigh–Taylor turbulence *Phys. Rev. E* **79** 065301
- [29] Chertkov M 2003 Phenomenology of Rayleigh–Taylor turbulence *Phys. Rev. Lett.* **91** 115001
- [30] Cabot W 2006 Comparison of two- and three-dimensional simulations of miscible Rayleigh–Taylor instability *Phys. Fluids* **18** 045101
- [31] Lafay M-A, Le Creurer B and Gauthier S 2007 Compressibility effects on the Rayleigh–Taylor instability between miscible fluids *Europhys. Lett.* **79** 64002
- [32] Gauthier S 2009 private communication
- [33] Le Creurer B and Gauthier S 2008 A return toward equilibrium in a 2D Rayleigh–Taylor instability for compressible fluids with a multidomain adaptive Chebyshev method *Theor. Comput. Fluid Dyn.* **22** 125
- [34] Tritton D J 1987 *Physical Fluid Dynamics* (Oxford: Clarendon)
- [35] Rast M P 1998 Compressible plume dynamics and stability *J. Fluid Mech.* **369** 125–49
- [36] Milovich J L, Amendt P, Marinak M and Robey H 2004 Multimode short-wavelength perturbation growth studies for the National Ignition Facility double-shell ignition target designs *Phys. Plasmas* **11** 1552–68
- [37] Abarzhi S I, Cadjan M and Fedotov S 2007 Stochastic model of Rayleigh–Taylor turbulent mixing *Phys. Lett. A* **371** 457
- [38] Abarzhi S I, Gorobets A and Sreenivasan K R 2005 Rayleigh–Taylor turbulent mixing of immiscible, miscible and stratified fluids *Phys. Fluids* **17** 081705
- [39] Celani A, Mazzino A and Vozella L 2006 Rayleigh–Taylor turbulence in two dimensions *Phys. Rev. Lett.* **96** 134504
- [40] Celani A, Matsumoto T, Mazzino A and Vergassola M 2002 Scaling and universality in turbulent convection *Phys. Rev. Lett.* **88** 054503
- [41] Ristorcelli J R and Clark T T 2004 Rayleigh–Taylor turbulence: self-similar analysis and direct numerical simulations *J. Fluid Mech.* **507** 213
- [42] Cabot W H and Cook A W 2006 Reynolds number effects on Rayleigh–Taylor instability with possible implications for type-Ia supernovae *Nat. Phys.* **2** 562
- [43] Livescu D 2003 Compressibility effects on the Rayleigh–Taylor instability growth between immiscible fluids *Phys. Fluids* **16** 118
- [44] George E and Glimm J 2005 Self-similarity of Rayleigh–Taylor mixing rates *Phys. Fluids* **17** 054101
- [45] Vladimirova N and Chertkov M 2009 Self-similarity and universality in Rayleigh–Taylor, Boussinesq turbulence *Phys. Fluids* **21** 015102
- [46] Boffetta G, Mazzino A, Musacchio S and Vozella L 2010 Statistics of mixing in three-dimensional Rayleigh–Taylor turbulence at low Atwood number and Prandtl number one *Phys. Fluids* **22** 035109